ADVANCED MATERIALS

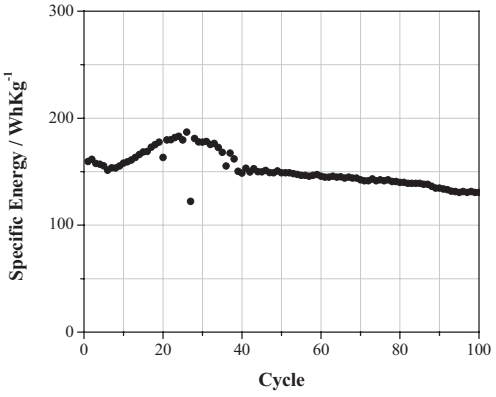

Figure 7. Energy density versus cycle number of a HPB/EC:DEC:$LiClO_4$/$LiMn_2O_4$ three-electrode cell at 25 °C and a *C*/5 rate. The energy density is calculated on the basis of the anode and cathode mass only.

different times, and iii) cooling to room temperature in 12 h. The products were removed from the walls of the ampoules, extracted with refluxing THF to eliminate the soluble parts, if any, and dried under reduced pressure (10^{-3} mbar). For simplicity, the final product is hereafter referred to as HPB carbon.

The physical, chemical, and morphological characteristics of the HPB carbon were checked by X-ray diffraction (XRD) and by scanning electron microscopy (SEM, Oxford Instruments LEO 1450VP). XRD experiments were carried out by means of a Phillips X'Pert Pro diffractometer, using Cu Kα radiation (2θ range 10°–60°, step size 0.05°, time/step 7.2 s).

The HPB carbon was ball-milled for a fixed period of time (10 min) to improve its morphology in view of electrode performance. For the electrochemical tests, the HPB was prepared in the form of a thin-film electrode (0.1 mm) by doctor-blade casting of a slurry of HPB, poly(vinylidene difluoride) [PVdF, binder], and fine Super P powder (electronic additive) onto a copper foil current collector [10]. Lithium manganese spinel, $LiMn_2O_4$, was prepared by solid-state synthesis using a stoichiometric amount of $LiOH{\cdot}H_2O$ (Aldrich, 99.5 %) and MnO_2 (Aldrich, 92 %). The reagents were first mixed in n-hexane, then the dried precursor was treated two times at 800 °C for 12 h in air and finally ground in an agate mortar. The structure was checked by X-ray diffraction. The Li/Mn ratio, measured by inductively coupled plasma (ICP) emission spectroscopy, was found to be 0.98/2.

A procedure similar to that described for the HPB electrodes was used for the preparation of thin-film $LiMn_2O_4$ electrodes, using aluminum foil as the current collector.

The capacity delivery and the cycle life of the HPB electrodes was investigated in electrochemical cells using a lithium metal counter electrode and as the electrolyte 1 M $LiClO_4$ in EC/DEC 1:1 in molar ratio. Laboratory two-electrode-type or coin-type cells were used. Cells were cycled in the voltage range 20–3000 mV at *C*/5 current rate (related to theoretical capacity of graphite).

The lithium-ion batteries were prepared by contacting in sequence a HPB anode, a Whatman fiberglass separator disk soaked with the liquid electrolyte (1 M $LiClO_4$ in EC/DEC 1:1 in molar ratio) and the $LiMn_2O_4$ cathode. The spinel/carbon ratio was 9:1 w/w. A third lithium metal reference was added. The cells were initially activated with a few cycles versus lithium metal electrode (*C*/5 current rate, 20–3000 mV) and then sealed for the remaining cycling tests. The latter were performed using a MACCOR 220 automatic battery cycler, in the voltage range 1000–4000 mV at *C*/5 current rate.

Received: June 25, 2004
Final version: October 12, 2004

[1] M. B. Armand, J. M. Tarascon, *Nature* **2001**, *414*, 359.
[2] B. Scrosati, in *Advances in Lithium-Ion Batteries* (Eds: W. van Schalkwijk, B. Scrosati), Kluwer–Plenum, New York **2002**, Ch. 6.
[3] F. Croce, G. B. Appetecchi, L. Persi, B. Scrosati, *Nature* **1998**, *394*, 456.
[4] S. Megahead, B. Scrosati, *J. Power Sources* **1994**, *51*, 79.
[5] R. A. Huggins, in *Handbook of Battery Materials*, Part III (Ed: J. O. Besenhard), Wiley-VCH, Weinheim, Germany, **1999**, Ch. 4.
[6] J. Yang, M. Winter, J. O. Besenhard, *Solid State Ionics* **1996**, *90*, 281.
[7] F. Croce, S. Panero, B. Scrosati, M. Wachtler, *J. Power Sources* **2004**, *129*, 90.
[8] M. Winter, J. O. Besenhard, *Electrochim. Acta* **1999**, *45*, 31
[9] T. Zheng, J. R. Dahn, in *Carbon Materials for Advanced Technologies* (Ed: T. D. Burchell), Pergamon, Amsterdam **1999**, Ch. 11, pp. 341–387.
[10] T. Renouard, L. Gherghel, M. Wachtler, F. Bonino, B. Scrosati, R. Nuffer, C. Mathis, K. Müllen, *J. Power Sources* **2005**, *139*, 242.
[11] M. Inagaki, *New Carbons: Control of Structure and Functions*, Elsevier Science, Oxford, UK **2000**.
[12] R. Fong, U. von Sachen, I. R. Dahn, *J. Electrochem. Soc.* **1990**, *137*, 2009.
[13] M. Winter and J. O. Besenhard, in *Lithium Ion Batteries*, (Eds: M. Wakihara and O. Yamamoto), Wiley-VCH,Weinheim, Germany, **1998**, Ch. 6, 127–155.

Tin/Platinum Bimetallic Nanotube Array and its Electrocatalytic Activity for Methanol Oxidation**

By *Yu-Guo Guo*, *Jin-Song Hu*, *Hui-Min Zhang*, *Han-Pu Liang*, *Li-Jun Wan*,* and *Chun-Li Bai**

Considerable attention has been paid to direct methanol fuel cells (DMFC) because of their potential use in powering portable electronic devices.[1–5] An effective electrocatalyst is the key component in DMFC. Although metal particles such as Pt and Pt–Ru are very useful in the anodic oxidation of methanol, high costs limit their practical application. Therefore, economical and effective alternative catalysts are required, and cost-effective routes are being sought to make more efficient Pt catalysts. One approach to achieve this aim is to produce Pt catalysts as nanoparticles with a high surface area for high catalytic performance and utilization efficiency.

[*] Prof. Dr. L.-J. Wan, Prof. Dr. C.-L. Bai, Dr. Y.-G. Guo, J.-S. Hu, Dr. H.-M. Zhang, H.-P. Liang
Institute of Chemistry, Chinese Academy of Sciences (CAS)
Beijing 100080 (P.R. China)
E-mail: wanlijun@iccas.ac.cn; clbai@iccas.ac.cn
Dr. Y.-G. Guo, J.-S. Hu, H.-P. Liang
Graduate School of CAS
Beijing 100064 (P.R. China)

[**] Financial support from the National Natural Science Foundation of China (No. 20025308 and 20177025), the National Key Project on Basic Research (Grant G2000077501) and the Chinese Academy of Sciences is gratefully acknowledged.

  DOI: 10.1002/adma.200400486

Recently we have shown that enhanced electrocatalysts of Pt can be obtained as hollow nanospheres without changing catalyst loading.[6] Another approach is to use Pt alloys to replace pure Pt. Among these alloy catalysts, Pt–Sn nanoparticles have been demonstrated as an attractive candidate reported by Wrighton's[7–10] and Golabli's groups.[11] They found that the activity of electrodeposited Pt–Sn bimetallic particles for methanol oxidation is not only higher than that of Pt particles,[10] but also higher than that of the acknowledged Pt–Ru particles.[11] On the other hand, the miniaturization of fuel cells requires submicrometer-sized conductive support electrodes. Therefore, single-walled and multiwalled carbon nanotubes have been recently used to support Pt clusters with a high surface area for developing electrode materials for DMFC,[12–15] in addition to the often-used electrically conducting carbon film. However, the synthesis, metal loading, and deposition of these nanotubes remain 1 non-trivial tasks. Recent efforts to prepare ordered arrays of metallic nanotubes by the template synthesis method pioneered by Martin's group, have provided new avenues to design high-surface-area electrode materials.[16–18] Highly ordered and well-aligned metallic nanotube arrays with a conductive substrate constitute a new class of submicrometer-sized conductive support electrodes. As the template synthesis method is a versatile approach, various metallic nanotube arrays can be fabricated for the consideration of electrodes. Here, we report our recent results on the study of catalysts. In order to produce a catalyst for DMFC with low cost and high efficiency, we have extended our previous research and improved the Pt–Sn nanoparticles to Pt–Sn nanotubes. An ordered and well-aligned array of Sn/Pt nanotubes was fabricated by a template synthesis method. The nanotube array showed remarkable activity toward methanol oxidation.

The Sn nanotube array serves as a conductive dispersing support for depositing Pt nanoparticles and promotes catalytic activity toward methanol oxidation. A schematic diagram of the procedure used to fabricate the Sn/Pt bimetallic nanotube array is shown in Figure 1. An evaporating and an electrodeposition process are used. Details of the fabrication are described in the Experimental section.

Figure 2a,b show the typical scanning electron microscopy (SEM) images of Sn nanotube arrays prepared by the evaporating process. It can be clearly seen that an ordered array of nanotubes with uniform diameter and length is formed. The hollow nature of the tubes is also confirmed by a transmission electron microscopy (TEM) image as shown in Figure 2c. The outer diameter of the nanotubes is ca. 300 nm, retaining the size and near cylinder shape of the pores of the anodic aluminum oxide (AAO) template.[19] The inner diameter of the nanotubes is ca. 210 ± 60 nm obtained by the high-magnification SEM image in Figure 2b. The average length of the Sn nanotubes is up to 60 μm (i.e., the entire thickness of the AAO template) according to cross-section SEM images of the array, indicating that the evaporated tin atoms have coated the pore wall in the entire channel of the AAO template. Furthermore, there are apparently no macroscopic defects in the nanotubes.

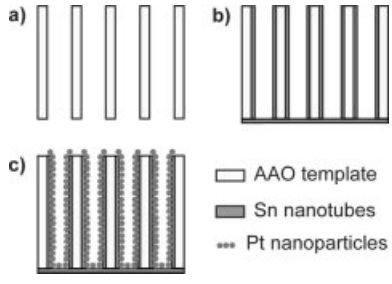

Figure 1. Schematic illustration of the procedure used to fabricate the Sn/Pt bimetallic nanotube array in the pores of a porous anodic aluminum oxide (AAO) template.

After electrodeposition of Pt, the morphology of the nanotube array was also characterized by SEM and TEM. Figure 2d shows a typical SEM image of the so-prepared Sn/Pt bimetallic nanotube array. It can be seen that a hollow structure is still retained, although the inner diameter of the nanotubes is smaller than that of pure Sn nanotubes. From a comparison of the TEM images of the Sn nanotube in Figure 2c and that after the electrodeposition of Pt in Figure 2e, it is clear that the wall thickness becomes larger after the electrodeposition. The inset in Figure 2e is a high-magnification TEM image of the Sn/Pt nanotube, showing the Pt nanoparticles on the inner-wall surface of the Sn nanotube.

The chemical composition of the bimetallic nanotubes is determined using energy-dispersive X-ray (EDX). In the EDX profile of the Sn/Pt nanotubes (Fig. 2f) the peaks of Sn and Pt are seen, confirming the successful deposition of platinum into the tin nanotubes. Quantitative analysis results show an atomic composition of 61.9 % Sn and 38.1 % Pt of the composite nanotubes.

The crystal structure of the Sn/Pt nanotubes was investigated by X-ray diffraction (XRD). Figure 3 shows the XRD pattern recorded for a Sn/Pt nanotube array. The eight diffraction peaks appearing at $2\theta = 30.7$, 32.1, 43.9, 45.0, 55.4, 62.6, 63.9, and 64.7° can be assigned as the 200, 101, 220, 211, 301, 112, 400, and 321 indices of the tetragonal phase of β-Sn, and the three main diffraction peaks appearing at $2\theta = 39.8$, 46.2, and 67.5° can be assigned as the 111, 200, and 220 indices of face-centered-cubic (fcc) Pt polycrystallites. Furthermore, the sizes of the Pt crystallites in the nanotubes are estimated from the widths of the major diffraction peaks observed in Figure 3 by Scherrer's formula. The mean crystallite size of D_{111} along the [111] axis is ca. 8.5 nm.

It is well known that the electrocatalytic activity of a catalyst is strongly dependent on its composition, size, surface area, and surface morphology.[3,20,21] To obtain a high surface area, catalysts are prepared as nanoparticles by techniques such as electrodeposition. Furthermore, it has also been found that the efficiency of catalysts, even of the same composition, is related to the morphology and distribution of the catalyst because of the diffusion of reactants and products during the reaction process.[22,23] To understand the morphology of the electrodeposited Pt, we used SEM and AFM to examine the

ADVANCED MATERIALS

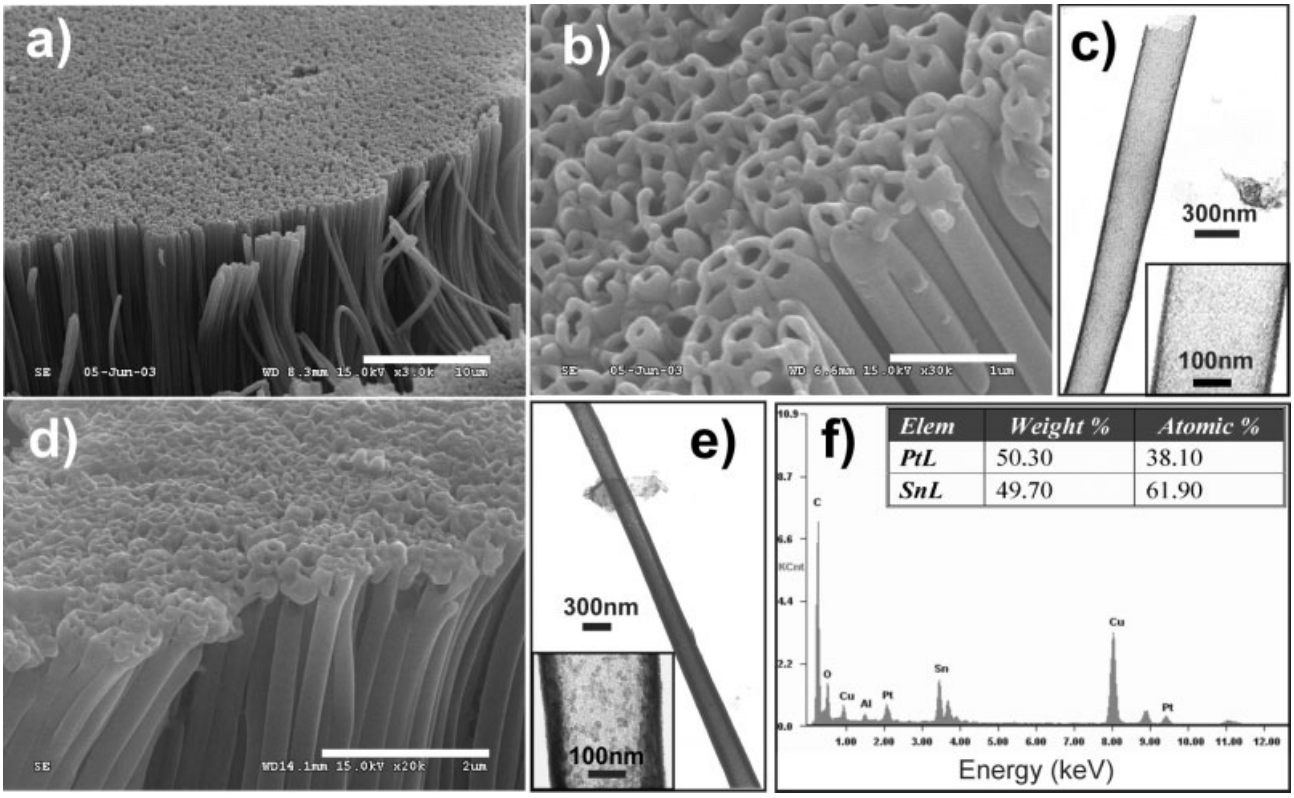

Figure 2. a,b) Typical SEM images of Sn nanotube arrays prepared by evaporating tin onto porous AAO template. c) Typical TEM image of a Sn nanotube. The inset shows the high-magnification TEM image of the Sn nanotube. d) Typical SEM images of a Sn/Pt bimetallic nanotube array prepared by electrodeposition of platinum into Sn nanotubes. e) Typical TEM image of a Sn/Pt bimetallic nanotube. The inset high-magnification TEM image in (e) shows the feature of Pt nanoparticles inlaying the inner-wall surface of the Sn nanotube. f) EDX (energy-dispersive X-ray) profile of the Sn/Pt nanotube shown in (e). Cu peaks are from the supporting copper grid.

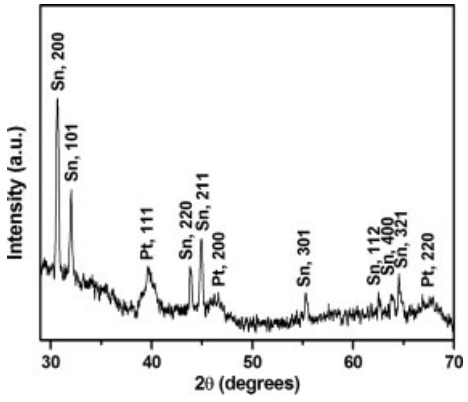

Figure 3. The XRD pattern of the Sn/Pt nanotube array. The result confirms the existence of tetragonal β-Sn and face-centered-cubic Pt.

changes that occur as the platinum layer is generated by electrodeposition on the underlying Sn substrate.

These experiments were carried out on planar Si wafers. The same procedure for the Sn and Pt layers as that used in the preparation of Sn and Sn/Pt nanotubes is employed. Figure 4a shows the SEM image of the Sn layer. An almost smooth surface is clearly seen. However, a dramatic change in morphology occurs after the electrodeposition of Pt onto the Sn layer, as shown in Figure 4b. The surface roughness increases dramatically with the appearance of Pt nanoparticles. The EDX profile of the surface of the composite film also revealed the presence of Pt and Sn. This is in good agreement with the previously reported Pt nanoparticles formed during the similar electrodeposition of platinum.[24] The results suggest that Pt nanoparticles form and inlay on the surface of the Sn layer. Because the characterization by SEM requires the covering of the surface of a specimen with a thin conduction film to prevent charging effects, which may hide some fine details of its surface features, we used AFM to investigate the Si/Sn/Pt film. From a typical AFM image (Fig. 4c), it is clearly seen that the Pt particles are on the nanoscale with a diameter of 30 ~ 80 nm, which is larger than those in the Sn nanotubes (ca. 20 nm obtained from the TEM image and ca. 8.5 nm estimated from the XRD data). The difference in particle size may be ascribed to the variety in the morphology and surface area between the Sn-nanotube-array electrode and the Sn-film electrode. Note that the sizes of particles observed by topographic AFM images are usually larger than their real sizes because of the influence of the size of the AFM tips. Therefore, the real size of the Pt particles in the film should be smaller than the observed diameter.

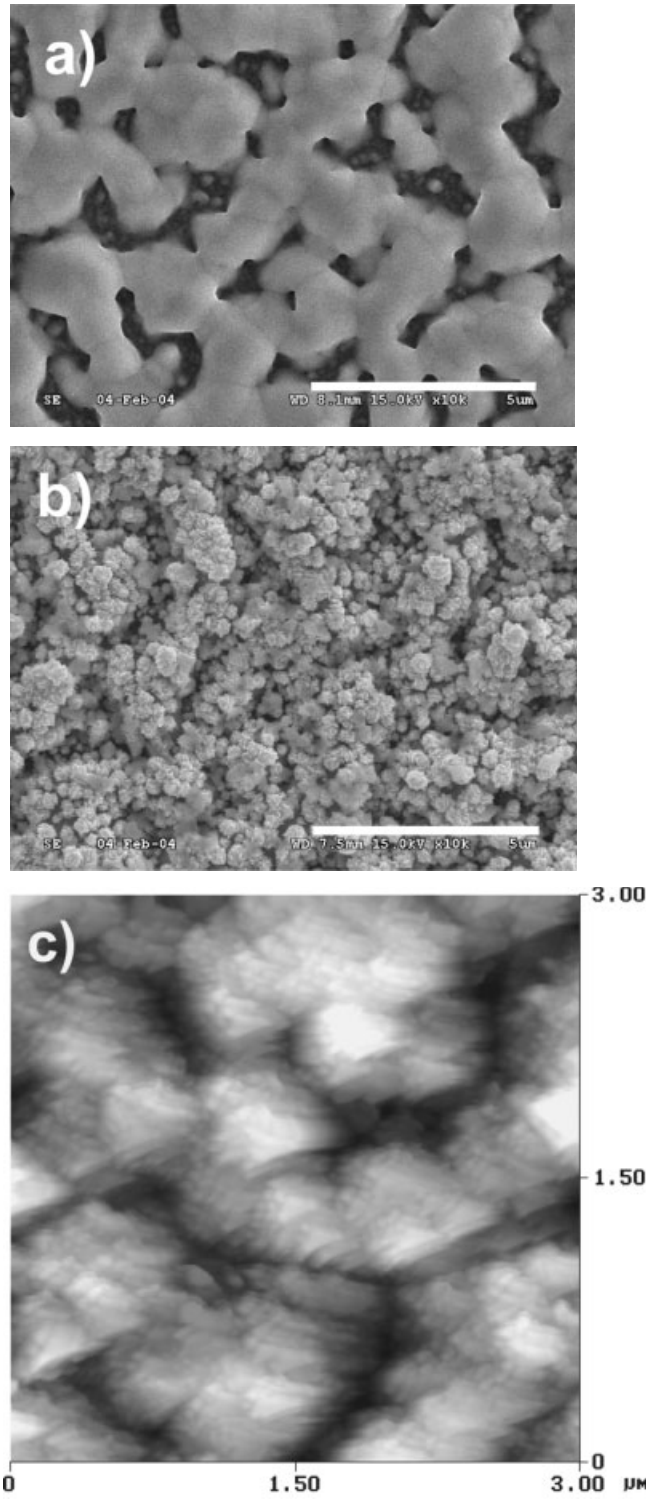

Figure 4. a) Representative SEM image of an Sn film prepared by evaporating tin onto an Si wafer. b) SEM and c) AFM images of an Sn/Pt film prepared by electrodeposition of platinum onto a Sn film.

The electrocatalytic activity of the Sn/Pt bimetallic nanotube array for the oxidation of methanol was investigated and compared with that of the Sn/Pt film on Si wafer by using a common electrochemical reaction in a solution of H_2SO_4.[5,25] Both of the electrodes were prepared by the same procedure and had the same geometric area of 0.785 mm^2. Cyclic voltammograms (CVs) are shown in Figure 5 for both electrodes in the absence and presence of 10 % MeOH in 0.5 M H_2SO_4. It can be clearly seen that both the Sn/Pt nanotubes and the nanofilms show catalytic behavior for the electro-oxidation of

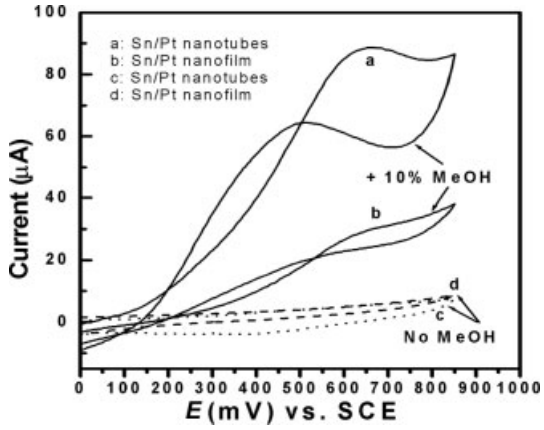

Figure 5. Cyclic voltammograms of Sn/Pt-bimetallic-nanotube and Sn/Pt-nanofilm electrodes in 0.5 M H_2SO_4 + 10 % MeOH (a,b) and in 0.5 M H_2SO_4 without MeOH (c,d), respectively. The geometric area of both electrodes was 0.785 mm^2. The scan rate was 50 $mV\,s^{-1}$.

methanol by the appearance of an oxidation current in the positive potential region. The onset of current attributed to methanol oxidation is at approximately 0.1 V (vs. a scanning calomel electrode (SCE)), which is more negative than that at a pure Pt electrode (ca. 0.3 V vs. SCE).[10] The negative shift is similar to that found for Pt–Sn alloy nanoparticles, indicating that the Sn/Pt composite has a positive effect on promoting the oxidation of methanol by lowering its overpotentials.[7–10] The peak potentials for the oxidation of methanol are around 0.65 V (vs. SCE) for both electrodes, in agreement with the literature value.[5,25] The peak currents of the Sn/Pt nanotube and the Sn/Pt nanofilm are 88.5 and 29.4 μA, respectively. It is clear that the catalytic activity of the Sn/Pt nanotubes is about twice higher than that of the Sn/Pt film. The remarkably high oxidation current for the Sn/Pt nanotubes may be directly related to the high electroactive surface areas of Pt nanoparticles. Since Sn nanotubes have nanochannel structures, a larger electroactive electrode surface area has been obtained than that of the planar Sn surfaces with the same geometric area. The higher surface area of Sn electrodes not only results in better dispersion of Pt nanoparticles on the Sn surfaces, but in the decrease of the size of Pt nanoparticles as shown in Figure 2e and Figure 4c. Therefore, the Sn/Pt nanotubes show a higher catalytic activity than that for the Sn/Pt films with the same Pt loading. In addition, the maximum anodic current of the Sn/Pt nanotube array with a Pt loading of 0.051 $mg\,cm^{-2}$, estimated from the cathodic charge

ADVANCED MATERIALS

passed corresponding to the reduction of Pt^{IV} to Pt^0, is up to 11.3 mA cm^{-2}, which is about five times higher than that of the reported C_{60}/Pt composite (ca. 1.8 mA cm^{-2}) with a similar Pt loading of 0.054 mg cm^{-2}.[26]

In summary, we have demonstrated that the electrodeposition of Pt nanoparticles into Sn nanotubes provides a simple and convenient method to design effective electrode materials for DMFC. The so-prepared composite nanostructures contain a large number of Pt nanoparticles inlaying the inner-wall surfaces of the Sn nanotubes. The novel structure results in a better dispersion of Pt nanoparticles with smaller size and hence endows it with a higher electroactive surface area of Pt. Electrocatalytic oxidation of methanol at the Sn/Pt-bimetallic-nanotube-array electrode shows remarkably enhanced activity compared with that at the Sn/Pt-film electrode. In addition, the Sn/Pt-composite nanotubes promote the oxidation of methanol by lowering its overpotential to that found at Pt–Sn alloy nanoparticles. It will be feasible to design the structure, size, and composition of the composite nanotube. Experiments are underway to further improve the performance of the Sn/Pt-nanotube-array electrode by introducing cost-effective Pt hollow nanospheres[6] or by depositing Pt nanoparticles on the outer surfaces of the Sn nanotubes, and to determine the underlying mechanism for the improved performance. The results described in the present report also demonstrate the ability of metallic nanotube arrays to serve as a new type of conductive support for fuel cell applications. Owing to its rich surfaces and easy manipulation, the composite structure will find use in a number of applications such as fuel cells, sensors, and chemical analysis.

Experimental

Tin foil (99.9 %) was obtained from Alfa. H_2PtCl_6 and MeOH were obtained from Beijing Chemical Reagent Ltd Co. Porous anodic aluminum oxide (AAO) membranes were commercially available from Whatman.

The Sn/Pt bimetallic nanotube array was fabricated by the procedure schematically shown in Figure 1. First, a layer of Sn (the preset thickness for the coating thickness meter was ca. 200 nm) was evaporated onto one side of the AAO membrane using a DZ-400 evaporating system at an evaporating rate of 0.4 Å s^{-1}) and under a high vacuum of $\sim 8.5 \times 10^{-5}$ Pa. The AAO membrane was positioned with pores normal to the evaporating target. The metal evaporant of tin formed under high vacuum will not cover (i.e., plug) the pores but will penetrate into the pores and deposit onto the pore walls. After the evaporation, another layer of Sn with the preset thickness of ca. 100 nm was subsequently evaporated at a fast evaporating rate (3 Å s^{-1}) and under a low vacuum of $\sim 3.5 \times 10^{-4}$ Pa. The metal nanoparticles formed in this condition will become larger and consequently cover and seal the pores, which results in the formation of a continuous film of Sn on the surface of the AAO template to provide a conductive contact.

For the incorporation of platinum nanoparticles into the Sn nanotubes and the subsequent electrocatalytic characterization of the so-prepared Sn/Pt nanotube electrode array, a specially constructed cell was used, consisting of a planar gold base onto which the Sn-coated membrane was placed. This base was screwed into a Teflon cell, with a 0.785 mm^2 O-ring to ensure sealing, a platinum wire counter electrode, and a saturated calomel electrode (SCE) as the reference electrode. Platinum nanoparticles were loaded into the Sn nanotubes embedded in the AAO films by cycling the Sn-nanotube/AAO electrodes in a solution containing 22.5×10^{-3} M H_2PtCl_6 between 0.0 and –0.9 V (vs SCE) at a scan rate of 20 V s^{-1}.

The removal of nanotubes from the AAO matrix was carried out by dissolving the AAO template in 4 M NaOH for 6 h to expose a freely standing array of nanotubes. For TEM observation, the nanotube arrays were ultrasonically dispersed in water and then dropped on carbon-coated copper grids. A Hitachi S-4300F field emission scanning electron microscope and a JEOL JEM-2010 transmission electron microscope operated at 200 kV and equipped with an energy-dispersive X-ray (EDX) analyzer (Phoenix) were employed in the study of the morphology and composition of the nanotubes. X-ray powder diffraction (XRD) was carried out on a Rigaku D/max-2500 using filtered Cu Kα radiation.

For comparison, Sn/Pt nanofilms were fabricated on planar Si wafers through the same procedure as that for the Sn/Pt nanotubes, and investigated by a Nanoscope IIIa scanning probe microscope (Digital Instruments) with a tapping mode, in addition to SEM. The electrocatalytic oxidation of methanol at the Sn/Pt-nanotube-array electrode and at the Sn/Pt nanofilms was carried out in a 0.5 M H_2SO_4 solution with 10 % methanol by using an EG&G PAR Basic Electrochemical System.

Received: March 30, 2004
Final version: November 9, 2004
Published online: January 24, 2005

[1] S. Wasmus, A. Kuver, *J. Electroanal. Chem*. **1999**, *461*, 14.
[2] T. Schultz, S. Zhou, K. Sundmacher, *Chem. Eng. Technol*. **2001**, *24*, 1223.
[3] A. T. Bell, *Science* **2003**, *299*, 1688.
[4] D. R. Rolison, *Science* **2003**, *299*, 1698.
[5] S. M. Golabi, A. Nozad, *J. Electroanal. Chem*. **2002**, *521*, 161.
[6] H.-P. Liang, H.-M. Zhang, J.-S. Hu, Y.-G. Guo, L.-J. Wan, C.-L. Bai, *Angew. Chem. Int. Ed*. **2004**, *43*, 1540.
[7] M. J. González, C. T. Hable, M. S. Wrighton, *J. Phys. Chem. B*. **1998**, *102*, 9881.
[8] M. J. González, C. H. Peters, M. S. Wrighton, *J. Phys. Chem. B*. **2001**, *105*, 5470.
[9] C. T. Hable, M. S. Wrighton, *Langmuir* **1993**, *9*, 3284.
[10] C. T. Hable, M. S. Wrighton, *Langmuir* **1991**, *7*, 1305.
[11] S. M. Golabi, A. Nozad, *Electroanalysis* **2003**, *15*, 278.
[12] H. L. Maynard, J. P. Meyers, *J. Vac. Sci. Technol. B*. **2002**, *20*, 1287.
[13] Z. L. Liu, X. H. Lin, J. Y. Lee, W. Zhang, M. Han, L. M. Gan, *Langmuir* **2002**, *18*, 4054.
[14] B. Rajesh, K. R. Thampi, J. M. Bonard, B. Viswanathan, *Bull. Mater. Sci*. **2000**, *23*, 341.
[15] G. L. Che, B. B. Lakshmi, C. R. Martin, E. R. Fisher, *Langmuir* **1999**, *15*, 750.
[16] M. Wirtz, C. R. Martin, *Adv. Mater*. **2003**, *15*, 455.
[17] C. R. Martin, D. T. Mitchell, *Electroanal. Chem.* **1999**, *21*, 1.
[18] H. Bayley, C. R. Martin, *Chem. Rev*. **2000**, *100*, 2575.
[19] H. Masuda, K. Fukuda, *Science* **1995**, *268*, 1466.
[20] A. J. Dickinson, L. P. L. Carrette, J. A. Collins, K. A. Friedrich, U. Stimming, *Electrochim. Acta* **2002**, *47*, 3733.
[21] N. Lopez, J. K. Norskov, *J. Am. Chem. Soc*. **2002**, *124*, 11 262.
[22] A. S. Eppler, G. Rupprechter, E. A. Anderson, G. A. Somorjai, *J. Phys. Chem. B*. **2000**, *104*, 7286.
[23] H.-M. Zhang, Y.-G. Guo, L.-J. Wan, C.-L. Bai, *Chem. Commun*. **2003**, 3022.
[24] K. Shimazu, K. Uosaki, H. Kita, Y. Nodasaka, *J. Electroanal. Chem*. **1988**, *256*, 481.
[25] K.-W. Park, J.-H. Choi, Y.-E. Sung, *J. Phys. Chem. B*. **2003**, *107*, 5851.
[26] K. Vinodgopal, M. Haria, D. Meisel, P. Kamat, *Nano Lett*. **2004**, *4*, 415.

